



Morphology-dependent structural and optical properties of ZnO nanostructures

Sonalika Agarwal¹ · Lokesh K. Jangir¹ · Kuldeep S. Rathore² · Manoj Kumar¹ · Kamlendra Awasthi¹

Received: 31 March 2019 / Accepted: 11 June 2019 / Published online: 24 July 2019
© Springer-Verlag GmbH Germany, part of Springer Nature 2019

Abstract

Zinc oxide nanostructures with three different morphologies, namely, nanoparticles (NP), nanorods (NR) and nanosheets (NS) were synthesized using chemical co-precipitation method. X-ray diffraction patterns showed that all the ZnO nanostructures had hexagonal wurtzite structures. The average crystallite size of NP, NS, and NR was found to be 25, 27 and 35 nm, respectively. The morphology and size of nanostructures were confirmed by scanning electron microscopy and transmission electron microscopy. The optical properties of zinc oxide nanostructures were investigated using UV–Vis absorption spectroscopy and photoluminescence (PL) spectroscopy. The optical band gap was found to be 3.26, 3.24 and 3.10 eV for NP, NS, and NR nanostructures, respectively. It was clearly observed from the PL spectrums that luminescence intensity was maximum for NP in the UV region and maximum for NS in the visible region. It is evident from the results that by changing the size and morphology of ZnO nanostructures, the optical properties can be tuned according to their desired applications.

1 Introduction

Semiconductor nanostructures of desired dimension and morphology have attracted a lot of interest and are widely used in the construction of optoelectronic devices [1, 2]. Zinc oxide (ZnO) has been recognized as one of the most important *n*-type II–VI semiconductors, with a direct wide band gap (3.37 eV) and has large exciton binding energy (60 MeV) [3, 4].

Additionally, ZnO is an interesting chemically and thermally stable semiconductor with hexagonal wurtzite structure having the ability to grow self-organized nanostructures in a wide range. Among the whole family of wide bandgap semiconductors nanostructures, ZnO has had the highest varieties of morphologies [5]. ZnO nanostructures are extensively used in a variety of applications such as near-ultraviolet emission, light emitting diodes, photovoltaic devices, solar cells, gas sensors, piezoelectric devices, transparent

electrodes and photocatalyst [6–10]. The optoelectronic properties of ZnO nanostructures were strongly affected by many parameters like morphology, size, crystallinity, defects, and impurity contents [10, 11]. The band-gap and luminescent properties can be tuned by changing the size and shape of ZnO nanostructures in the near ultra-violet and visible regions [12, 13].

Recently, Al-Gaashani et al. [14] investigated the optical properties of the ZnO nanostructures of various morphologies prepared by microwave-assisted aqueous solution method and showed that the biggest crystallite size of ZnO nanostructures has the lowest band gap energy. Musa et al. [15] synthesized ZnO nanorods of one dimension with various lengths and diameters. They observed that by increasing growth time the diameter and length of nanorods also increase. Furthermore, it is observed from PL spectrum that the intensity of emission bands considerably depends on the length of ZnO nanorods. The peak of the UV band is increased when the length of the ZnO nanorods is decreased. Also, Yang et al. [11] studied the effect of the morphology of ZnO nanostructures on the optical properties. The red shift has been observed from the PL spectra at the position of a UV emission peak due to change in the morphology of ZnO nanostructures from nanorods arrays to rod particle. Therefore, the optical properties of nanostructures depend on their morphologies.

✉ Sonalika Agarwal
sonalika.spsl@gmail.com

✉ Kamlendra Awasthi
kawasthi.phy@mmit.ac.in

¹ Department of Physics, Malaviya National Institute of Technology Jaipur, Rajasthan 302017, India

² Department of Physics, University of Rajasthan, Jaipur 302004, India

Several physical methods have been used to prepare ZnO nanostructures of different morphologies like pulsed laser deposition [2], chemical vapor deposition [16], solvothermal [17], sol-gel synthesis [18], hydrothermal route [19] and chemical co-precipitation [20]. Among the other methods, chemical co-precipitation method is a suitable method due to its reproducibility, simplicity, purity and low cost for large-scale production [21, 22].

In this paper, ZnO nanoparticles, nanorods and nanosheets have been successfully synthesized using a simple chemical co-precipitation method to investigate their morphological influence on the optical properties. The synthesized samples were characterized by X-ray diffraction (XRD), scanning electron microscopy (SEM) and transmission electron microscopy (TEM), and optical properties were studied using UV-visible absorption spectroscopy and photoluminescence spectroscopy (PL).

2 Experimental details

2.1 Materials

Zinc nitrate hexahydrate ($\text{Zn}(\text{NO}_3)_2 \cdot 6\text{H}_2\text{O}$) ($\geq 96\%$), Merck), sodium hydroxide (NaOH) (97%, Fisher Scientific), hexamethylenetetramine (HMT) (99%, Merck), ethanol and deionized (DI) water were used as received without any further purification.

The chemical co-precipitation method was adopted for the synthesis of different morphologies of ZnO, namely nanoparticles (NP), nanorods (NR) and nanosheets (NS).

2.2 Synthesis of ZnO nanoparticles

For the synthesis of ZnO nanoparticles, a solution (A) of 2.2 g of $\text{Zn}(\text{NO}_3)_2 \cdot 6\text{H}_2\text{O}$ in 40 mL of DI water was prepared under constant stirring at 90 °C. Another solution (B) of 8 g NaOH in 40 mL DI water was prepared. 8 mL of solution (B) was added dropwise to solution A, and the resultant milky white solution (C) was continually stirred for 2 h. This resultant solution was kept overnight to settle down the nanoparticles. After that, the desired product was centrifuged and washed with DI water for five times. After complete washing, ZnO nanoparticles were dried at 60 °C for 24 h and then it changed into powder form [23].

2.3 Synthesis of ZnO nanorods

In a typical experiment, two aqueous solutions (A) and (B) were prepared. First, solution (A) was prepared in 100 mL of DI water by dissolving of 2.97 g $\text{Zn}(\text{NO}_3)_2 \cdot 6\text{H}_2\text{O}$, whereas the second solution (B) was ready in the same amount of DI water by dissolving 1.40 g HMT. Further, solutions (A) and

(B) were mixed under mild magnetic stirring for 5 min. The resultant solution was placed in an oven at 90 °C for 24 h [24]. Then, the solution was centrifuged and washed with DI water many times for removing the impurities and dried at 60 °C for 24 h. Finally, ZnO nanorods were obtained in powder form.

2.4 Synthesis of ZnO nanosheets

ZnO nanosheets were prepared by the following same procedure with some modification in the method of synthesized ZnO nanoparticles. The process of preparing solutions A, B and C was the same at room temperature. Now, this solution C was kept at 90 °C for 24 h in the oven. The resulting hot solution with a white precipitate was left to cool down to RT naturally. Then, the white precipitate was separated by centrifugation and washed with DI water several times, and dried in air at 60 °C for 24 h to obtain in powder form.

3 Methods

The XRD patterns of the ZnO nanostructures were recorded at room temperature by Panalytical XPert Pro X-ray diffractometer using $\text{Cu-K}\alpha$ radiation source at $\lambda = 1.5406 \text{ \AA}$. The morphology and particle size of the samples were examined with field emission scanning electron microscopy (FESEM, Nova Nano FE-SEM 450 FEI) and high-resolution transmission electron microscopy [HRTEM, Tecnai G² 20 (FEI) S-TWIN]. Optical absorption spectrums were recorded by UV-visible spectrophotometer (UV-Vis, LAMBDA 750 Perkin Elmer) in the wavelength range of 200–800 nm to calculate the band gap of ZnO nanostructures. To investigate the luminescence properties and possible defects, room temperature photoluminescence spectrums were recorded by LABHR-UV-EVO, using He-Cd laser with 30 mW of power, at 325 nm excitation wavelength.

4 Results and discussion

The crystallinity and crystal phase of the ZnO nanostructures (NP, NR, and NS) were studied by XRD patterns as shown in Fig. 1. It is clearly observed from Fig. 1 that all diffraction patterns were same excluding the variation in the intensities of the peaks due to the change in the morphologies. All the diffraction peaks can be easily indexed to the pure hexagonal wurtzite phase of ZnO. Additionally, in the spectrums, no characteristic peaks were noticed related to the other impurities, indicating that ZnO was prepared with high purity. Table 1 shows the lattice parameters, JCPDS card no. and crystallite average size of all the ZnO samples. The average crystallite sizes of NP, NR, and NS were

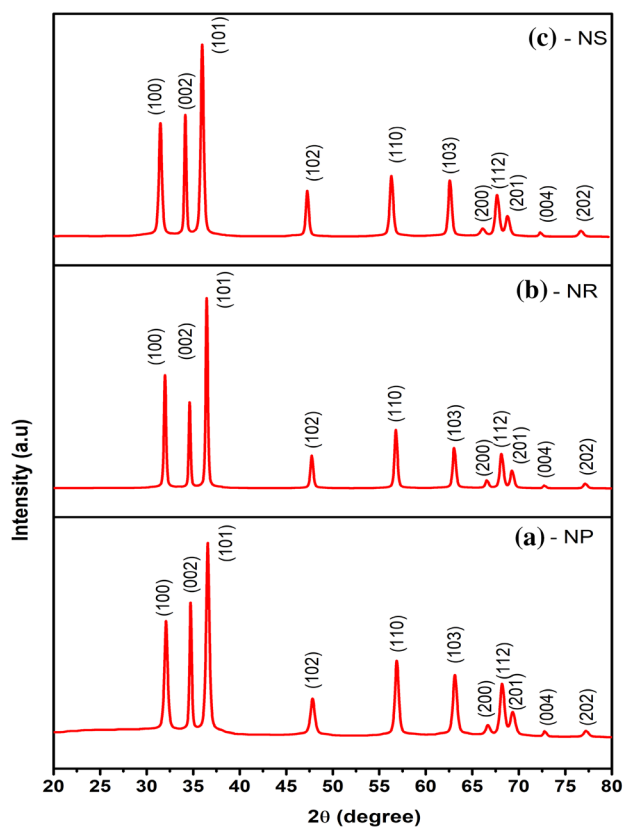


Fig. 1 XRD patterns of different morphologies of ZnO. **a** NP **b** NR and **c** NS

calculated by Debye Scherer's formula and found 25, 27 and 35 nm, respectively.

Figure 2a–c shows the typical magnified FESEM images of the as-synthesized samples with different morphology. A large quantity of semi-spherical ZnO nanoparticles (NP) with an average size of ≈ 30 nm were observed from Fig. 2a. Figure 2b shows uniformly distributed ZnO nanorods with a diameter in the range of 100–400 nm, whereas the average length of the nanorods is about several micrometers. It is also revealed that ZnO nanorods have hexagonal

cross-section structure with a fine and smooth surface and formed of chalk-like morphology (shown in inset). Figure 2c demonstrates that the SEM image of microstructures is composed of sheet-like morphology. Mostly, the nanosheets are linked to each other and form networks, which do not show well-ordered patterns, and their sizes vary from 1 to 5 μm . The thickness of the nanosheets is in the range of 15–30 nm.

For further confirmation of the nanostructure, particle size and crystallinity, the TEM and HRTEM images were also recorded. Figure 2d–f shows the typical low magnification TEM images of the prepared ZnO nanostructures (NP, NR, and NS) and is in good agreement with the results obtained from the SEM. Figure 2d displays dispersed and uniform ZnO nanoparticles (NP) with the semi-spherical shape. The average particle size of the nanoparticles was found to be 25 nm. The rod-like structure can be clearly seen from the TEM image (Fig. 2e). The diameter of nanorods is about 80–150 nm and the length is in the micrometer range. Figure 2f shows the TEM image of nanosheets, which are assembled non uniformly. These nanosheets seem agglomerated due to the intersection with each other. The average thickness of the nanosheets was found to be in the range of 16–32 nm. The HRTEM images, shown in Fig. 2g–i, confirms the existence of crystalline ZnO nanoparticles, nanorods, and nanosheets, respectively. The measured interplanar distances are 0.261 nm, 0.244 nm, and 0.241 nm, which correspond to (002) (101) and (101) planes for wurtzite ZnO NP, NR, and NS, respectively, as shown in Table 1, which is in good agreement with the XRD results.

Figure 3 shows the UV–Vis absorption spectra of different morphologies of ZnO nanostructures (NP, NR, and NS). In the absorption spectra, the peaks are certified to the electrons transitions between the intrinsic defect levels and between the valence band and conduction [25]. It can be seen from Fig. 3a that the maximum absorbance is observed for nanoparticles (NP). The main absorption peaks at room temperature for ZnO NP (25 nm), NR (35 nm) and NS (27 nm) are around 362 nm, 375 nm, and 367 nm, respectively, shown in the inset of Fig. 3. Therefore, in the

Table 1 The lattice parameters, JCPDS card no., crystallite average size, interplanar distance and planes of different morphologies of ZnO nanostructures

S. no.	ZnO samples name	Morphology	Lattice parameters	JCPDS card no.	The average crystallite size (nm)	Measured interplanar distances from HRTEM (nm)	Interplanar distances from XRD (nm)	Corresponding planes from XRD
1	NP	Nanoparticles	$a = b = 3.245 \text{ \AA}$, $c = 5.200 \text{ \AA}$	01-079-0205	25	0.261	0.259	(002)
2	NR	Nanorods	$a = b = 3.244 \text{ \AA}$, $c = 5.197 \text{ \AA}$	01-079-0205	35	0.244	0.246	(101)
3	NS	Nanosheets	$a = b = 3.2487 \text{ \AA}$, $c = 5.202 \text{ \AA}$	01-079-0205	27	0.241	0.246	(101)

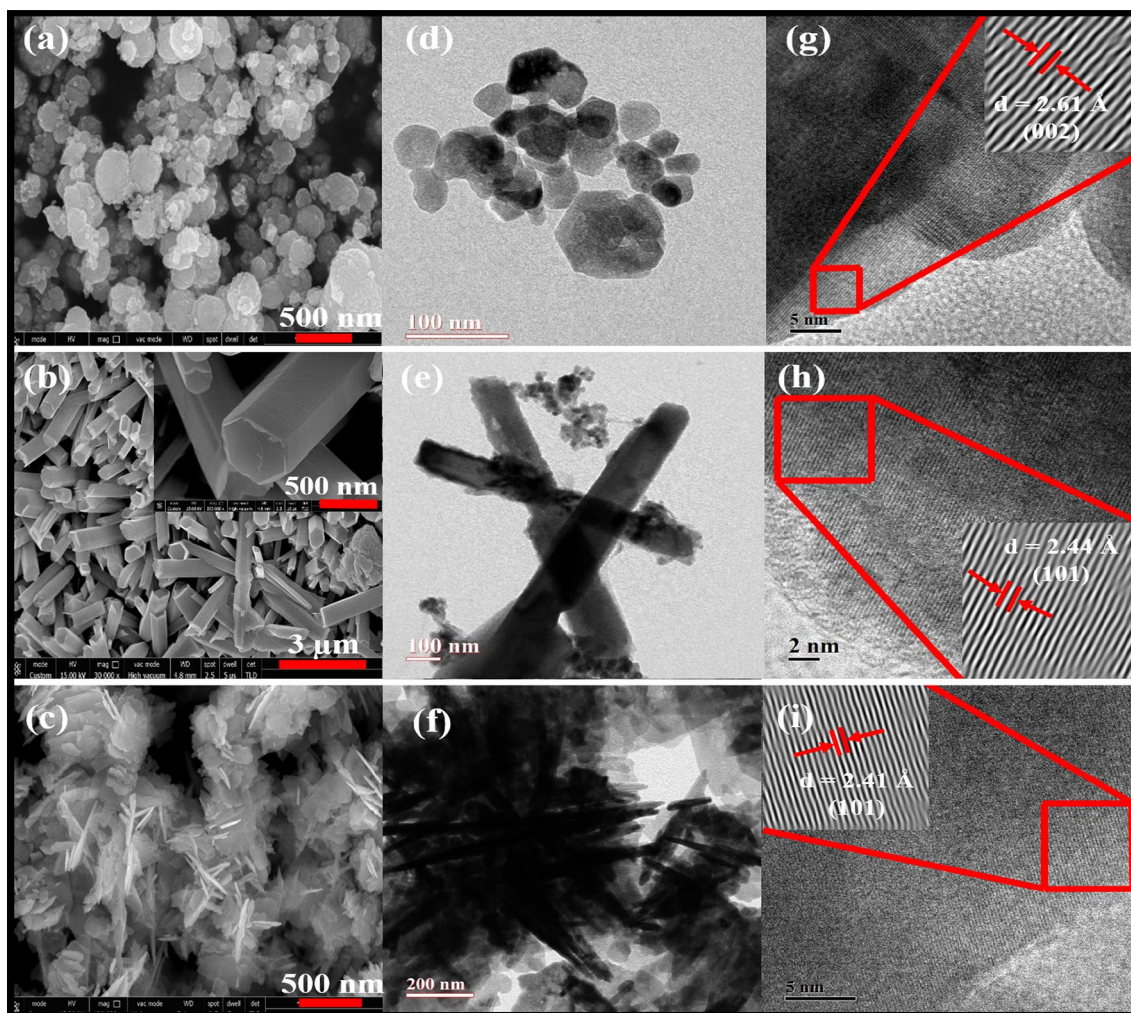


Fig. 2 a–c SEM images of ZnO NP, NR, and NS; d–f TEM images of ZnO NP, NR, and NS and g–i HRTEM images of NP, NR, and NS, respectively, showing lattice fringes of ZnO

characteristic absorption peaks, a blue shift was clearly observed with a decrease in crystallite size of the nanostructures [26, 27]. The blue shift can be mainly attributed to the Burstein–Moss (BM) effect [28, 29], which is commonly observed in *n*-type semiconductors. This blue shift could be related to the decrease in size and quantum confinement effects [30], due to the blockage of low energy transitions [31, 32] and the changes in surface morphology [12, 33].

The optical band gap (E_g) was calculated using Tauc's equation as follows [34]:

$$\alpha h\nu = A (h\nu - E_g)^n,$$

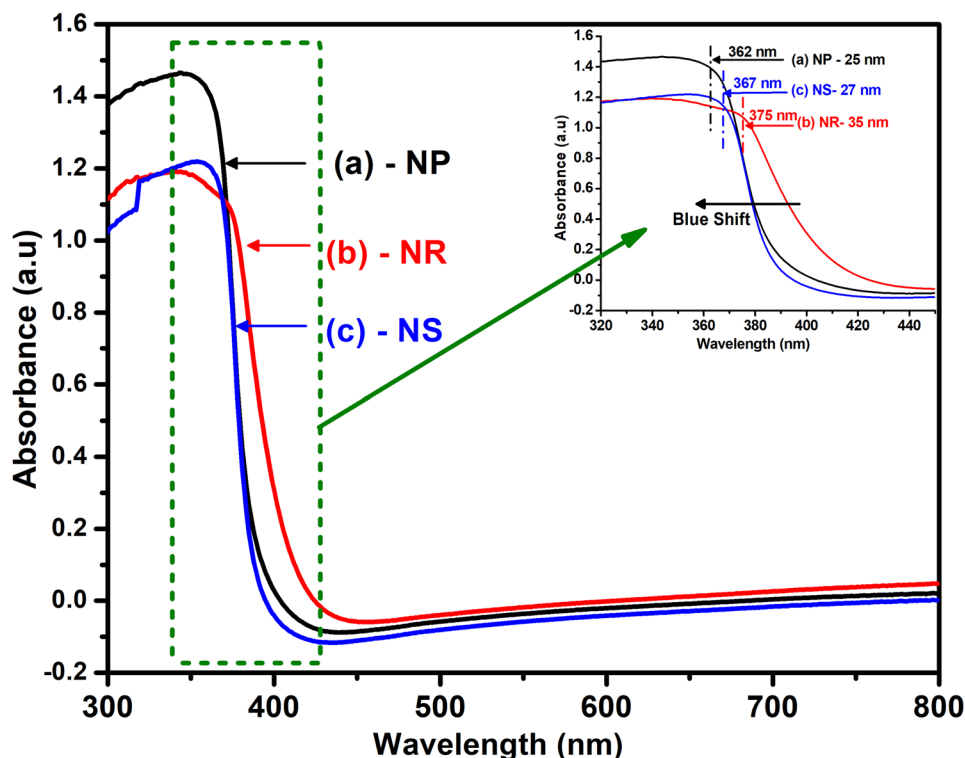
where α is the absorption coefficient, A is a constant, $h\nu$ is the photon energy, E_g is the optical band gap energy and n is $\frac{1}{2}$ for a direct semiconductor.

The graphs were plotted between $(\alpha h\nu)^2$ and photon energy ($h\nu$) for all samples and shown in Fig. 4a–c for (NP,

NR, and NS) ZnO nanostructures, respectively, to determine the value of energy band gap. The values of the energy band gap obtained for NP, NR and NS are 3.26, 3.10 and 3.24 eV, respectively. It is observed that the energy band gap is size dependent and increases with a decrease in crystallite size of ZnO nanostructure due to the optical confinement effect [35, 36]. It is also revealed that the band gap is strongly affected by the size, morphology as well as synthesis methods of ZnO nanostructures [33]. This behavior of E_g could be explained on the basis of surface-related defects and/or adsorbed species [36, 37]. The obtained results of band gap are in good agreement with the previous literature of ZnO nanostructures [38–40].

The room temperature photoluminescence (PL) spectrums of the ZnO nanostructures were recorded at an excitation wavelength of 325 nm and shown in Fig. 5. From all the PL spectrums (Fig. 5), two dominant emission bands were observed, one with less intense UV emissions in the range

Fig. 3 UV–Vis absorption spectra of different morphologies of ZnO. **a** NP, **b** NR, and **c** NS and in the inset (blue shift)



of 350–400 nm and another with broad intense visible emissions from 450 to 700 nm. The first emission band, which is in the UV region attributed to the near-band-edge emission resulting from the recombination of free excitons through an exciton–exciton collision process [41, 42]. In addition, the second emission band is a broad, deep level emission in the visible region [43]. The visible emission is generally associated with various point defects, intrinsic defects and extrinsic defects, e.g., oxygen vacancies, zinc interstitials and the incorporation of hydroxyl groups in the crystal lattice located at the surface of the material, and is formed during the preparation of nanostructures [44–46]

Further, to determine the crystal quality of material, UV luminescence was used whereas to evaluate structural defects, visible luminescence might be used [47]. In the present study, the UV emission peak of ZnO nanoparticles is sharper and stronger than that of rod-like and sheet-like nanostructures, indicating that the ZnO nanoparticles have better crystal quality with good optical properties. Besides this, the broad emission around 560 nm (for NP) is usually signified as the green emission, while two other broad emissions at near 610 nm (for NR and NS) are referred to as orange emission. The green emission is normally referred to singly ionized oxygen vacancies resulting from the radiative recombination of a photogenerated hole with an electron occupying the oxygen vacancy. The orange–red emission band is related to oxygen interstitials (O_i) originates from the point defects, produced during the synthesis of material

[6, 7, 48]. Additionally, another interesting remark is that the emission peak intensity in the visible region increases when the morphology of ZnO nanostructures changed from nanoparticles to nanorods and to nanosheets. Therefore, the strongest luminescence intensity of ZnO nanosheets suggests that a larger fraction of oxygen vacancies due to the structural defects [11] makes it more suitable for photocatalytic and optoelectronic applications.

5 Conclusion

A facile chemical process has been revealed for the preparation of different morphologies of ZnO nanostructures. This method is proposed because it has numerous advantages like simplicity, cost-effective and moderate condition. The synthesized nanostructures have good structural and optical qualities. The XRD analysis revealed that the ZnO nanostructures are single crystalline with a wurtzite hexagonal phase. SEM and TEM images showed the variation in size and morphology of nanoparticles to rod-like and then to sheet-like structures, depending on the parameters and conditions during the synthesis process. The UV–Vis absorption results show a blue shift in the characteristic absorption peaks with a decrease in the crystallite size of the nanostructures. The optical band gap was calculated and was found to increase with a decrease in average crystallite size, attributed to the quantum confinement effect. It is also observed from

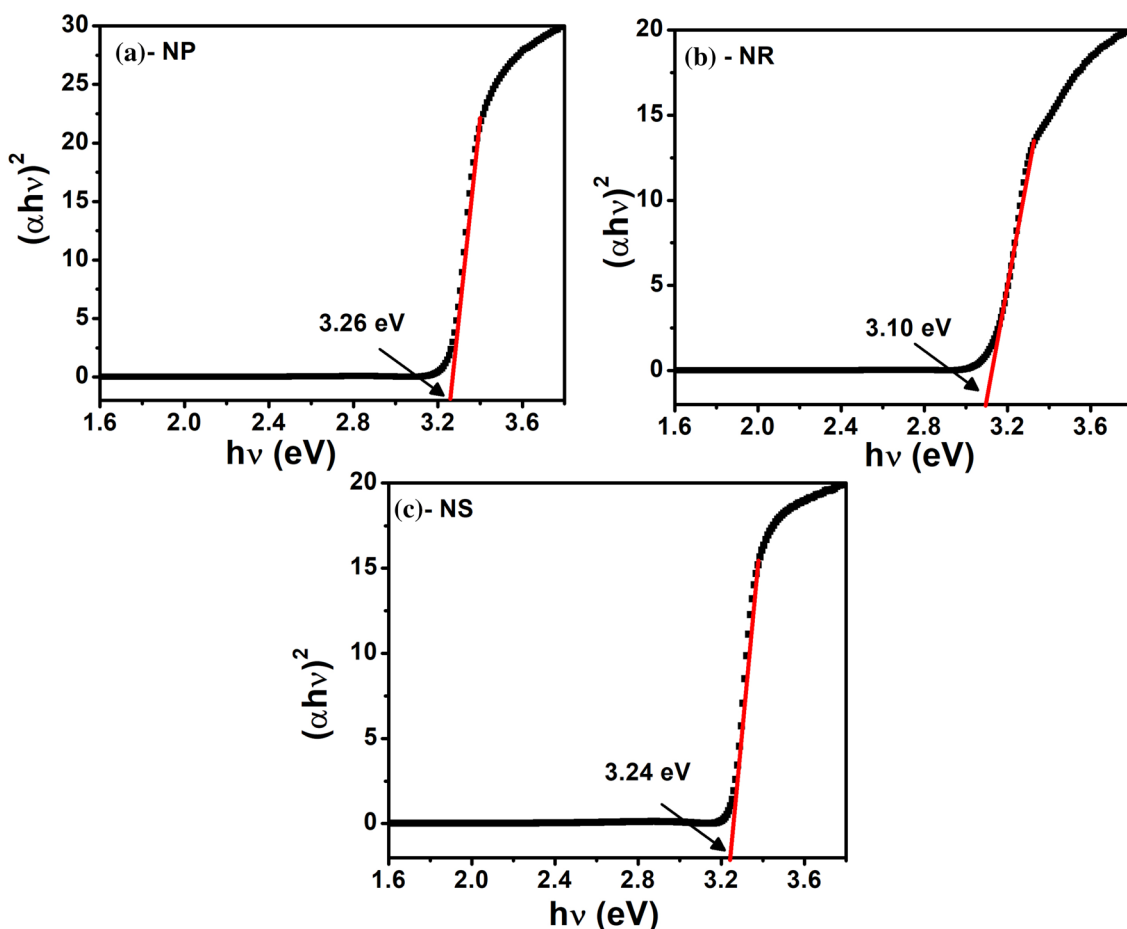


Fig. 4 The energy band gap of different morphologies of ZnO. **a** NP, **b** NR, and **c** NS estimated by the extrapolation of the linear part of $(\alpha h\nu)^2$ versus $h\nu$ plots

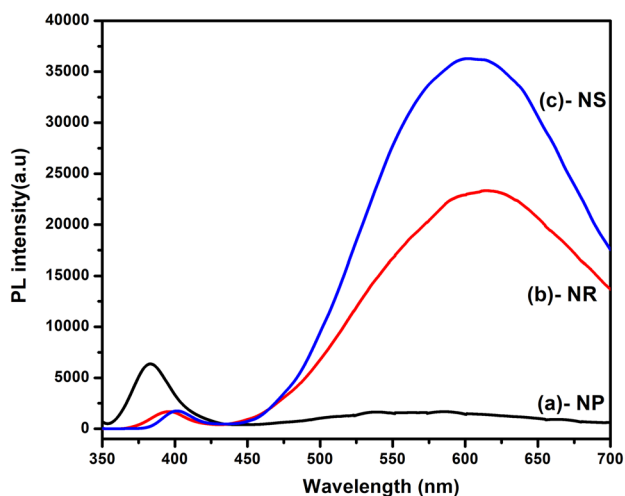


Fig. 5 Room temperature PL spectrum of different morphologies of ZnO. **a** NP, **b** NR, and **c** NS

the results that the optical properties are strongly affected by the size, morphology as well as by the synthesis methods of ZnO nanostructures. The PL study suggests that ZnO nanoparticles have better crystal quality than that of nanorods and nanosheets because of the strongest emission peak in the UV region. In addition, ZnO nanosheets showed the highest luminescence intensity peak in the visible domain than the nanoparticles and nanorods. Such type of behavior might be specifically interesting for many applications like in optoelectronic devices, display devices, sensing devices, etc.

Acknowledgements Sonalika Agarwal is very grateful to the Department of Science and Technology, Government of India for financial support vide reference no. SR/WOS-A/PM-72/2016 under Women Scientist Scheme to do this work. This work is also supported by DST, New Delhi under Grant no. ECR/2016/001780.

References

1. U. Pal, J.G. Serrano, P. Santiago, G. Xiong, K.B. Ucer, R.T. Williams, *Opt. Mater. (Amst)*. **29**, 65 (2006)

2. L. Feng, A. Liu, M. Liu, Y. Ma, J. Wei, B. Man, J. Alloys Compd. **492**, 427 (2010)
3. Y. Zhang, T. Liu, J. Hao, L. Lin, W. Zeng, X. Peng, Z. Wang, Appl. Surf. Sci. **357**, 31 (2015)
4. S. Kataria, S. Bala, S. Chand, S. Mahendia, OP Sinha, S. Kumar, in *AIP Conference Proceedings*, **2093**, p. 020031 (2019)
5. W. Zhang, X. Chen, N. Xu, R. Xiang, Y. Zhu, Z. Tang, J. Nanomater. **2013**, 5 (2013)
6. Q.J. Yu, W.Y. Fu, C.L. Yu, H.B. Yang, R.H. Wei, M.H. Li, S.K. Liu, Y.M. Sui, Z.L. Liu, M.X. Yuan, G.T. Zou, G.R. Wang, C.L. Shao, Y.C. Liu, J. Phys. Chem. C **111**, 17521 (2007)
7. H. Yeon, S. Han, T. Whan, Appl. Surf. Sci. **256**, 6117 (2010)
8. S. Kumar, P.D. Sahare, Opt. Commun. **285**, 5210 (2012)
9. S.S. Kumar, P. Venkateswarlu, V.R. Rao, G.N. Rao, Int. Nano Lett. **3**, 30 (2013)
10. S. Agarwal, P. Rai, E. Navarrete, E. Llobet, F. Güell, Sens. Actuators B. Chem. **292**, 24 (2019)
11. Z. Yang, Z. Ye, Z. Xu, B. Zhao, Phys. E Low Dimens. Syst. Nanostruct. **42**, 116 (2009)
12. R. Raji, K.G. Gopchandran, J. Sci. Adv. Mater. Devices **2**, 51 (2017)
13. J.H. Zhao, C.J. Liu, Z.H. Lv, Optik (Stuttg). **127**, 1421 (2016)
14. R. Al-gaashani, S. Radiman, A.R. Daud, N. Tabet, Y. Al-douri, Ceram. Int. **39**, 2283 (2013)
15. I. Musa, N. Qamhie, S.T. Mahmoud, Results Phys. **7**, 3552 (2017)
16. G.-C. Yi, C. Wang, W. Il Park, Semicond. Sci. Technol. **20**, S22 (2005)
17. D. Yiamsawas, K. Boonpavanitchakul, W. Kangwansupamonkon, J. Microsc. Soc. Thail. **23**, 75 (2009)
18. Y. Zhang, H. Jia, P. Li, F. Yang, Z. Zheng, Opt. Commun. **284**, 236 (2011)
19. P. Rai, J.N. Jo, I.H. Lee, Y.T. Yu, Mater. Chem. Phys. **124**, 406 (2010)
20. N.S. Rao, M.V.B. Rao, Am. J. Mater. Sci. **5**, 66 (2015)
21. M.K. Debanath, S. Karmakar, Mater. Lett. **111**, 116 (2013)
22. P.B. Taunk, R. Das, D.P. Bisen, J. Radiat. Res. Appl. Sci. **8**, 433 (2015)
23. L. Kumar Jangir, Y. Kumari, A. Kumar, M. Kumar, K. Awasthi, Mater. Chem. Front. **1**, 1413 (2017)
24. B. Zhang, W. Fu, X. Meng, A. Ruan, P. Su, H. Yang, Ceram. Int. **43**, 5934 (2017)
25. Q. Zhu, C. Xie, H. Li, C. Yang, S. Zhang, D. Zeng, J. Mater. Chem. C **2**, 4566 (2014)
26. S. Doris, G. Johannes, T.R. Klupp, V. Vassil, P. Wolfgang, ACS Nano **3**, 1703 (2009)
27. Y.H. Yang, X.Y. Chen, Y. Feng, G.W. Yang, Nano Lett. **7**, 3879 (2007)
28. B.E. Sernelius, K.-F. Berggren, Z.-C. Jin, I. Hamberg, C.G. Granqvist, Phys. Rev. B **37**, 10244 (1988)
29. A. Ghosh, R.N.P. Choudhary, J. Exp. Nanosci. **5**, 134 (2010)
30. Y. Gu, I.L. Kuskovsky, M. Yin, S. O'Brien, G.F. Neumark, Appl. Phys. Lett. **85**, 3833 (2004)
31. E. Burstein, Phys. Rev. **93**, 632 (1954)
32. R.N. Ali, K. Diao, H. Naz, X. Cui, B. Xiang, Mater. Res. Express **4**, 095015 (2017)
33. Y. Köseoğlu, Ceram. Int. **40**, 4673 (2014)
34. J. Tauc, A. Menth, J. Non Cryst. Solids **8–10**, 569 (1972)
35. B. Yang, A. Kumar, P. Feng, R.S. Katiyar, Appl. Phys. Lett. **92**, 233112 (2008)
36. K.L. Foo, U. Hashim, K. Muhammad, C.H. Voon, Nanoscale Res. Lett. **9**, 429 (2014)
37. J. Duraimurugan, G.S. Kumar, M.V.P. Maadeswaran, J. Mater. Sci. Mater. Electron. **29**, 9399 (2018)
38. K.-F. Lin, H.-M. Cheng, H.-C. Hsu, L.-J. Lin, W.-F. Hsieh, Chem. Phys. Lett. **409**, 208 (2005)
39. H. Kou, X. Zhang, Y. Du, W. Ye, S. Lin, C. Wang, Appl. Surf. Sci. **257**, 4643 (2011)
40. A. Nandi, R. Majumder, P. Nag, S.K. Datta, J. Mater. Sci. Mater. Electron. **28**, 10885 (2017)
41. K. Vanheusden, W.L. Warren, C.H. Seager, D.R. Tallant, J.A. Voigt, B.E. Gnade, J. Appl. Phys. **79**, 7983 (1996)
42. A. Umar, Y.B. Hahn, Nanotechnology **17**, 2174 (2006)
43. J.B. Baxter, F. Wu, E.S. Aydil, Appl. Phys. Lett. **83**, 3797 (2003)
44. R. Zhang, P.G. Yin, N. Wang, L. Guo, Solid State Sci. **11**, 865 (2009)
45. B.K. Meyer, H. Alves, D.M. Hofmann, W. Kriegseis, D. Forster, F. Bertram, J. Christen, A. Hoffmann, M. Straßburg, M. Dworzak, U. Haboeck, A.V. Rodina, Phys. Status Solidi **241**, 231 (2004)
46. D. Raoufi, J. Lumin. **134**, 213 (2013)
47. S. Mridha, D. Basak, Phys. Status Solidi **206**, 1515 (2009)
48. M. Liu, A.H. Kitai, P. Mascher, J. Lumin. **54**, 35 (1992)

Publisher's Note Springer Nature remains neutral with regard to jurisdictional claims in published maps and institutional affiliations.